Journal of Advanced Ceramics
2017, **6**(4): 312–319
https://doi.org/10.1007/s40145-017-0243-3
ISSN 2226-4108
CN 10-1154/TQ

Research Article

Upconversion $32Nb_2O_5$–$10La_2O_3$–$16ZrO_2$ glass activated with Er^{3+}/Yb^{3+} and dye sensitized solar cell application

Xiaoyu LI[a,†], Jiaying LI[a,b,†], Jianqiang LI[a,c,*], Hong LIN[d], Bo LI[b]

[a]*National Engineering Laboratory for Hydrometallurgical Cleaner Production Technology*, *Key Laboratory of Green Process and Engineering*, *Institute of Process Engineering*, *Chinese Academy of Sciences*, *Beijing 100190*, *China*
[b]*Advanced Materials Institute*, *Graduate School at Shenzhen*, *Tsinghua University*, *Shenzhen*, *Guangdong 518055*, *China*
[c]*University of Chinese Academy of Sciences*, *Beijing 100049*, *China*
[d]*State Key Laboratory of New Ceramics and Fine Processing*, *Department of Materials Science and Engineering*, *Tsinghua University*, *Beijing 100084*, *China*

Received: April 10, 2017; Revised: August 08, 2017; Accepted: August 22, 2017

Abstract: Er^{3+}/Yb^{3+} codoped niobium pentoxide glasses were fabricated by the aerodynamic levitation (ADL) method with rapid cooling rate. All samples with various doping concentrations showed good upconversion luminescence properties under 980 nm laser excitation. The structure, transmittance spectrum, and luminescence properties of the samples were systemically investigated by XRD, UV–Vis–NIR spectrophotometer, and upconversion spectra. All transparent samples exhibited green and red upconversion emissions centered at 532, 547, and 670 nm. Experimental results showed that the sample codoped with 1 mol% Er^{3+}/Yb^{3+} has the strongest upconversion emissions, and the increase of the doped Yb^{3+} concentration results in the increased red emission and reduced green emission. The log*I*–log*P* plot of green emission indicated that the green emissions reach the saturation at high pump power excitation, deviating from the low-power regime. After one-photon energy transfer (ET) process, $^4I_{11/2}+{}^4I_{11/2}\rightarrow{}^4F_{7/2}+{}^4I_{15/2}$ process between the two neighboring Er^{3+} ions was responsible for the population of the $^4S_{3/2}$/$^4H_{11/2}$ states. The niobium pentoxide codoped with Er^{3+}/Yb^{3+} bulk glasses could be used in the dye sensitized solar cell (DSSC) to improve the efficiency.

Keywords: aerodynamic levitation (ADL); niobium pentoxide; upconversion; rare earth concentration; solar cell

1 Introduction

Upconversion luminescence materials have been extensively investigated for their promising applications in the fields of solar cell, biological diagnosis, infrared detection, and solid state lasers, etc. [1–13]. Due to their special anti-Stokes process which converts the low-energy photon into high-energy photon, the upconversion luminescence has attracted great attention of scientists. Chen *et al*. [14] reported a photolithography via upconversion nanoparticle-assisted photochemistry. Qiao *et al*. [15] used the

†These authors contributed equally to this work.
*Corresponding author.
E-mail: jqli@ipe.ac.cn

upcoversion nanoparticles to detect of primary gastric tumor and lymphatic metastasis. Yuan *et al.* [16] achieved the improvement of the overall conversion efficiency of the dye sensitized solar cells by using the upconversion colloidal nanoparticles. However, the low upconversion efficiency limits the practical application of upconversion luminescence materials. Thus, it is significant to improve the upconversion efficiency by developing upconversion luminescence materials of new type and novel structure.

$NaYF_4$ has the highest upconversion luminescence efficiency at present, but its preparation process needs fluorinated raw materials which are harmful to the environment. What is more, its poor machinability and chemical stability limit the application of fluoride upconversion luminescence materials. The oxide matrix material is a high desirable candidate material for upconversion luminescence. Glassy or disordered hosts are preferred as active layers for highly efficient solar cell application. Non-uniform broadening in absorption spectra of rare earth (RE) ions permits absorbing a larger part of the solar spectrum owing to the disorder of the host [17]. Unlike the nanoparticles, bulk upconversion luminescence glass with good mechanical property has been used in solar cell [18]. Lahoz *et al.* [19] reported the application of Ho^{3+} doped glass–ceramic materials via direct melting glass to further improve the conversion efficiency of the Si solar cells. However, most of bulk upconversion glass/ceramic materials were fabricated by traditional melt-quenching. There is stretching vibration in the network structure of conventional glass-forming oxides such as silica, boron oxide, and phosphorus pentoxide. High phonon energy limits the high efficiency of upconversion luminescence of conventional oxides. And the container will cause the heterogeneous nucleation and contamination. Aerodynamic levitation (ADL) method is a promising technique to vitrify materials with low glass-forming ability into bulk form under the containerless condition. It could suppress the inhomogeneous nucleation and container wall's contact-pollution. Our previous work reported the La_2O_3–Nb_2O_5 bulk glass, which was hard to form by conventional processing method, was firstly prepared via ADL. The different Ta_2O_5 doping concentrations were studied at the same time [20]. Nb_2O_5 is used as network modifier, which has non-bridging oxygens [21] and contributes to host a content of rare earth ions. Niobium pentoxide is a candidate matrix material for efficient conversion of luminescence materials because the high valence of Nb_2O_5 is in favor of the upconversion of the rare earth elements. Taking into account its good machinability and chemical stability, Nb_2O_5 materials may have more promising future than fluorides on the application of the dye sensitized solar cell (DSSC).

In this study, we have fabricated an upconversion niobium pentoxide bulk glass codoped with various ratios and contents of Er^{3+}/Yb^{3+} by ADL. To enhance upconversion luminescence, the optimized concentration of the doped rare earth elements was found in our study. The limit of the doped rare earth elements concentration is related to the matrix network. Traditional network formers such as SiO_2 with network rigidity will result in the formation of clusters that are not suitable to host a high content of rare earth ions. In contrast, niobium pentoxide as the network modifier may have the advantage of obtaining higher codoping concentration [22,23]. The possible upconversion mechanism was systematically discussed. We also explored the application of bulk upconversion luminescence on DSSC. And the results indicate that bulk upconversion luminescence glass with good mechanical property can be used in solar cell.

2 Experimental

The raw materials were high-purity Nb_2O_5 (99.99 wt%), La_2O_3 (99.99 wt%), ZrO_2 (99.99 wt%), Yb_2O_3 (99.9 wt%), and Er_2O_3 (99.99 wt%) powders weighed in stoichiometric composition. The first step to optimize the concentration of rare earth elements was to explore the maximum codoped concentration. The compositions of Er^{3+}/Yb^{3+} codoped niobium pentoxide glass were $(Nb_{0.64}La_{0.2}Zr_{0.16})O_{2.22}$–$xYb_2O_3$–$2xEr_2O_3$ (x = 0.1, 0.2, 0.3, 1/3), and the obtained glass samples were labeled as NLZm (m = 1, 2, 3, 4) respectively. We also tried x = 0.4 (NLZ5), but the sample was opaque, thus it was not discussed below. Then under the total identical doping amount of 1 mol%, the samples with different proportion in rare earth elements were fabricated. The compositions of these bulk glasses were $(Nb_{0.64}La_{0.2}Zr_{0.16})O_{2.22}$–$yYb_2O_3$–$zEr_2O_3$ (y/z = 0.5:0.5, 1/3:2/3, 0.25:0.75, 0.2:0.8), and the obtained glass samples were labeled as NLZn (n = 6, 7, 8, 9) respectively. The detail contents of doped rare earth elements are shown in Table 1. Then the powders were mixed thoroughly in the agate mortar with small amount of ethanol added. After the process, the

mixtures were compressed into columnar rods. Then the rods were cut into small pieces with a mass of about 80 mg after they were sintered at 1100 ℃ for 10 h in a resistance. Subsequently, the small samples were fabricated into spherical glasses by an ADL furnace. During the process, the sample was levitating away from the nozzle at the gas flow rate of 1200 SCCM and melted under CO_2 laser of 80 W power for several seconds. After the laser power was turned off, the homogeneous melts of NLZ1–4 and NLZ6–9 were quenched into transparent solid spherical glasses with a diameter size of ~3 mm at an approximate cooling rate of 250 ℃/s. The details about ADL furnace have been introduced elsewhere [24,25]. A video camera with high-resolution charge-coupled device was applied to realize the magnified *in situ* observation of the samples. Simultaneously, infrared pyrometer (the temperature range from 278 to 2004 ℃) was employed to monitor the temperature of sample during the process at the laser emission rate of 0.8 [26]. Finally, for later measurements, the glass spheres were carefully polished into 1.5-mm-thick wafers or ground into powders.

The density of glass samples was measured by an Archimedes' method and all the data were an average of three experiments. The reflective index was determined by spectroscopic ellipsometry (SENTECH SE850). The detail content, density, and refractive index of doped rare earth elements are shown in Table 1. X-ray diffraction (XRD; Smartlab 9, Rigaku Corporation, Tokyo, Japan) was employed to identify the structure of the sample. The transmittance spectrum of the prepared wafer in wavelength from 350 to 2500 nm was recorded by a UV–VIS–NIR spectrophotometer (PERSEE TU-1901). Upconversion luminescence spectra were recorded by a spectrofluorometer (Fluorolog-3, Jobin Yvon, Paris, France) excited by a diode laser with 980 nm continuous wave (0.5–1500 mW power was used). The DSSC equipped with bulk niobium pentoxide upconversion glass was synthesized according to the procedure reported previously [27] and the whole device is shown in Fig. 9. The current–voltage (*I–V*) characteristics of the cells were measured with an AM 1.5 solar simulator (CEP-25TF, Bunkoukeiki Co., Ltd.). Data were collected by source meter (Keithley 2400).

Table 1 Composition, density, and refractive index of Er^{3+}/Yb^{3+} codoped NLZ1–9 glass samples

Sample	Yb_2O_3 (mol%)	Er_2O_3 (mol%)	Density of glass sample, ρ (g/cm^3)	Reflective index of glass sample at 632.8 nm, n	Total number of model photon emissions[b]
NLZ1	0.10	0.20	5.35	2.144	5.78×10^8
NLZ2	0.20	0.40	5.39	2.387	8.01×10^8
NLZ3	0.30	0.60	5.27	2.244	8.73×10^8
NLZ4[a]	0.33	0.66	5.61	2.287	8.89×10^8
NLZ6	0.50	0.50	5.86	2.242	1.10×10^9
NLZ7[a]	0.33	0.66	5.61	2.287	8.89×10^8
NLZ8	0.25	0.75	5.68	2.279	4.71×10^8
NLZ9	0.20	0.80	5.38	2.273	5.96×10^8

[a]NLZ4 and NLZ7 actually are the same composition. In order to compare the different rule of luminescence more clearly, we use the different number in two types of contrast discussion.
[b]The value is obtained by integrating the area of the curve in Fig. 3.

3 Results and discussion

Since the same properties are obtained in NLZ codoped with the different concentrations and proportions of Er^{3+} and Yb^{3+} ions, XRD patterns of the NLZ4 and NLZ9 as the typical samples of NLZ1–4 and NLZ6–9 were measured and shown in Fig. 1. Weak and broad diffraction bands are observed in the spectra. The XRD patterns indicate that NLZ1–4 and NLZ6–9 samples are amorphous-like NLZ glass [28].

Figure 2 shows the transmittance spectra of the NLZ bulk glass without Er^{3+}/Yb^{3+} and NLZ4 ranging from 350 to 2500 nm. Thickness of each sample is 1.5 mm. The transmittance of the pure matrix NLZ glass is below 70% and decreases rapidly in the visible region. The transmittance of the NLZ4 sample is about 70% in the visible region and increases to 76% in the near-infrared region. In the most visible and near-infrared region, the transmittance of the sample doped with Er^{3+}/Yb^{3+} is higher than that of the matrix. The good transmittance will cause the infrared light irradiating through the whole upconversion glass,

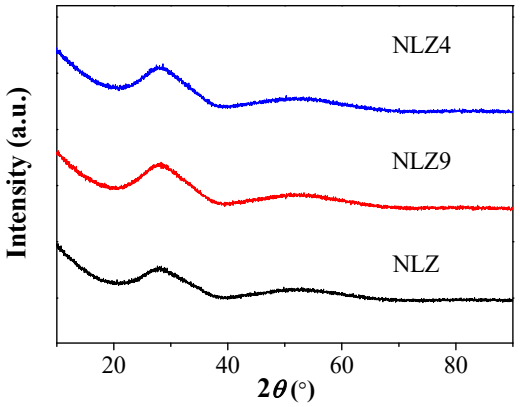

Fig. 1 Measured XRD patterns of powders NLZ, NLZ4, and NLZ9.

producing the upconversion light. Furthermore, the upconversion light can transmit the energy through the glass, which can be utilized by solar cells. As noted in Fig. 2, five obvious absorption peaks centered at 488, 522, 651, 790, and 1545 nm are assigned to the transitions from the $^4I_{15/2}$ ground state to the $^4F_{7/2}$, $^4H_{11/2}$, $^4F_{9/2}$, $^4I_{9/2}$, and $^4I_{13/2}$ excited states of Er^{3+} ions, respectively. The absorption peak centered at 978 nm is illustrated by the transitions $^4I_{15/2}\rightarrow{}^4I_{11/2}$ of Er^{3+} ions and $^2F_{7/2}\rightarrow{}^2F_{5/2}$ of Yb^{3+} ions.

Figure 3 displays the upconversion emission spectra of NLZ glass doped with different concentrations of Er^{3+} and Yb^{3+} ions under 980 nm laser excitation. The upconversion emission spectra of all samples doped with different concentrations of Er^{3+} and Yb^{3+} ions have two main peaks centered at 532 and 547 nm of $^4H_{11/2}/^4S_{3/2}\rightarrow{}^4I_{15/2}$ in the green emissions and one peak centered at 670 nm of $^4F_{9/2}\rightarrow{}^4I_{15/2}$ in the red emission.

As illustrated in Fig. 3, the red upconversion emissions are enhanced with the increasing concentration of Er^{3+} and Yb^{3+} ions, ranging from 0.3 to 1 mol% (NLZ1–4). Different from the increasing tendency of the intensities of red emissions, the green emissions of NLZ2, NLZ3, and NLZ4, which are centered at around 547 nm, are far more than the intensity of NLZ1. The spectra results show that it obeys the rule that the emission intensity is enhanced with the increase of the rare earth concentrations of both Er^{3+} and Yb^{3+} ions. We also calculated total green and red emitted photon numbers of all samples which are summaried in Table 1. Clearly NLZ6 codoped with 1 mol% Er^{3+} and Yb^{3+} ions shows the strongest upconversion luminescence. Insert of Fig. 3 is the digital image of NLZ6 sample under excitation of 0.25 mW 808 nm laser, and the green upconversion emission is strong to be seen by naked eyes. The red emission may be attributed to $^4I_{13/2}(Er^{3+}) + {}^4I_{11/2}(Er^{3+})\rightarrow{}^4F_{9/2}(Er^{3+}) + {}^4I_{15/2}(Er^{3+})$. And green emission is $^2F_{5/2}(Yb^{3+}) + {}^4I_{15/2}(Er^{3+})\rightarrow{}^2F_{7/2}(Yb^{3+}) + {}^4I_{11/2}(Er^{3+})$, $^4I_{11/2}(Er^{3+}) + {}^4I_{11/2}(Er^{3+})\rightarrow{}^4F_{7/2}(Er^{3+}) + {}^4I_{15/2}(Er^{3+})$. The cross relaxation (CR) process between the two neighboring Er^{3+} ions is responsible for the population of the $^4S_{3/2}/^4H_{11/2}$ states. However, the green emissions reach the "saturation" state when the concentration of codoped rare earth ions is larger than a certain threshold. In SiO_2 and other traditional networker formers, the rare earth element ion concentration can be increased, but unfortunately result in the formation of clusters due to the network rigidity of these glasses. In the glasses containing modified ions, the local environment of rare earth ions is defined preferentially by non-bridging oxygens [29]. In NLZ glass, Nb_2O_5 is used as network modifier, which has non-bridging oxygens [21] and contributes to the glass matrix to host a high content of rare earth ions.

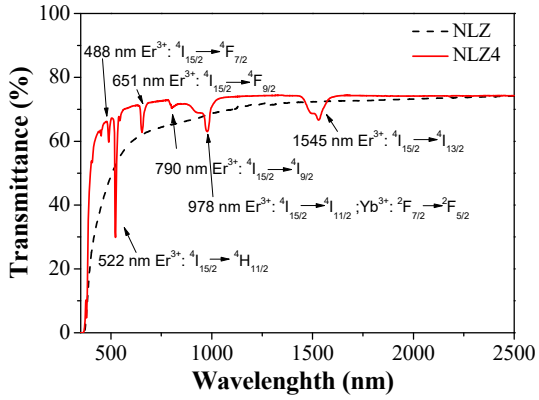

Fig. 2 Transmittance spectra of the undoped NLZ glass and doped NLZ4 sample.

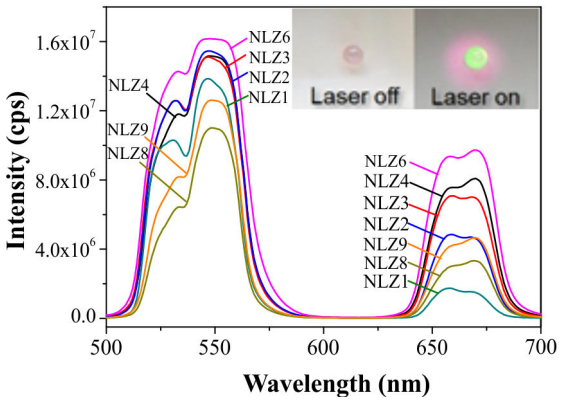

Fig. 3 Upconversion emission spectra of NLZ*m* (*m* = 1, 2, 3, 4, 6, 8, 9) glass samples at the excitation of 1.5 W 980 nm laser. Insert is the digital image of the NLZ6 sample under excitation of 0.25 mW 808 nm laser.

The upconversion process is a multi-photon process. The emission intensity (I) is proved to be a function of pump power (P) and the number of photon absorbed per photon emitted (n): $I \propto P^n$. The curves reported in the literature are linear [30,31]. The emission intensity depends on the pump power because that the low energy photons can be absorbed by Er^{3+} and Yb^{3+} ions in an "unsaturated" upconversion process. The luminescence mechanism is showed in Fig. 4, which has been illustrated in the previous work [21]. Some new phenomena occurred in our experiments. Figure 5 depicts that the log$I$–log$P$ plots of the red emission are linear and the slope values (it is the photon absorbed per photon emitted n in the formula above) are ranged from 1.88 to 2.24. n decreases with the increase of rare earth

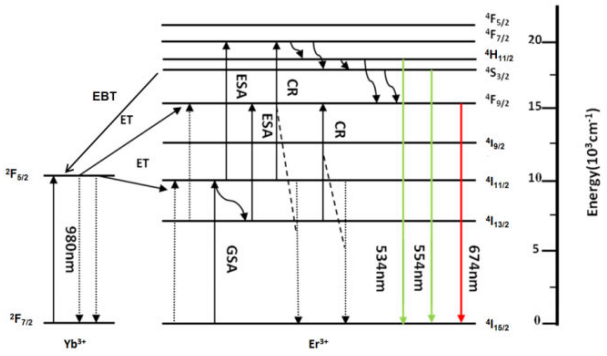

Fig. 4 Energy level diagram of Er^{3+} and Yb^{3+} in NLZ glass and possible mechanisms.

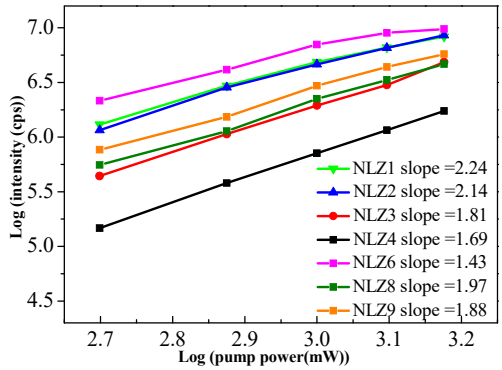

Fig. 5 Log–log plot of the red emission intensity versus the pump power of NLZ*m* (*m* = 1, 2, 3, 4(7), 6, 8, 9).

ion concentration for the CR process: $^4I_{13/2}(Er^{3+}) + {}^4I_{11/2}(Er^{3+}) \rightarrow {}^4F_{9/2}(Er^{3+}) + {}^4I_{15/2}(Er^{3+})$. The rate of CR process is proportional to $1/R^6$, where R means the distance between two neighboring Er^{3+} ions [29]. The increasing concentration of Er^{3+} ions shortens the distance between two neighboring Er^{3+} ions. Consequently, $^4F_{9/2}$ levels are more generated and red emissions enhance that lead to the reduction of absorbed photons.

However, the curve of log*I*–log*P* of green emission shows parabolic curve (Fig. 6). The curves in the low pump power are the linear lines with the slope values close to 2, and the line slope decreases (the number of photon absorbed per photon emitted is decreased) with the increase of pump power to 1500 mW. It indicates that the green light emissions saturate at high pump power excitation, deviating from the low-power regime [32,33].

The slope values become smaller in the green emissions for NLZ1–4, which may be attributed to the ET process. After one-photon ET process: $^2F_{5/2}(Yb^{3+}) + {}^4I_{15/2}(Er^{3+}) \rightarrow {}^2F_{7/2}(Yb^{3+}) + {}^4I_{11/2}(Er^{3+})$, $^4I_{11/2}(Er^{3+}) + {}^4I_{11/2}(Er^{3+}) \rightarrow {}^4F_{7/2}(Er^{3+}) + {}^4I_{15/2}(Er^{3+})$. The CR process between the two neighboring Er^{3+} ions is responsible for

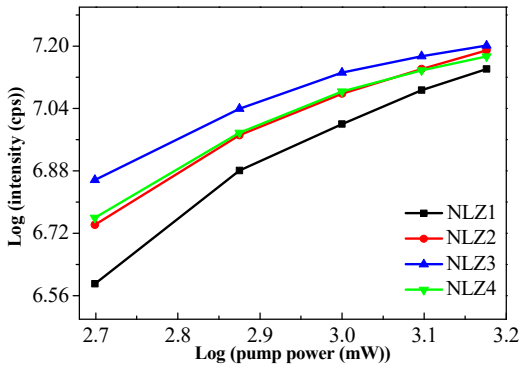

Fig. 6 Log–log plot of the green emission intensity versus the pump power of NLZ*m* (*m* = 1, 2, 3, 4).

the population of the $^4S_{3/2}/^4H_{11/2}$ states. This is because at high laser pump power, the efficient ET process will result in quantities of Er^{3+} ions at the $^4I_{11/2}$ state, and then the CR process occurs due to the long-lived $^4I_{11/2}$ state of Er^{3+} ions. The concentrations of rare earth ions also affect the mechanism of luminescence. For the reason that the distance between Yb^{3+} and Er^{3+} ions is shortened and attributed to the occurrence of energy back transfer (EBT) process. Green emission is the main luminescence mechanism and EBT is easy to be gained in the green emissions.

The upconversion luminescence of NLZ doped with 1 mol% concentration of Er^{3+} and Yb^{3+} ions expresses good performance thus we keep the total identical doping amount for the latter experiment. The samples with the same concentration of Er^{3+} and Yb^{3+} ions (codoped amount 1 mol%) but in different ratios have been tested. The log*I*–log*P* plot of the NLZ6–9 shows the parabolic curve in the green emissions in Fig. 7. The increased concentration of Yb^{3+} ions contributes to the absorption of photons in ET process: $^2F_{5/2}(Yb^{3+}) + {}^4I_{15/2}(Er^{3+}) \rightarrow {}^2F_{7/2}(Yb^{3+}) + {}^4I_{11/2}(Er^{3+})$, and the intensity of green emissions increases with increased addition

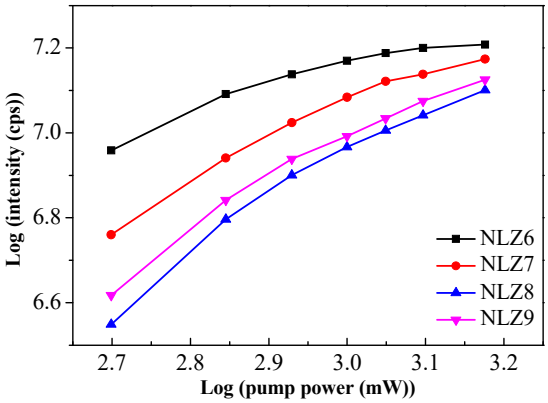

Fig. 7 Log–log plot of the green emission intensity versus the pump power of NLZ*n* (*n* = 6, 7, 8, 9).

amount of Yb^{3+} ions. The increase of the pump power and the photon numbers leads to the generation of $^4I_{11/2}$ and CR happens between two neighboring Er^{3+} ions, while the energy level of $^4F_{7/2}$ generates and emits green luminescence. The curve slope value decrease means the number of absorbed photon per emitted photon decreases with the increase of pump power.

The distances between the Er^{3+} and Yb^{3+} ions become shortened with the increased concentration of the Yb^{3+} ions. The shortening distance contributes to the increased rate of CR ($^4I_{13/2}(Er^{3+}) + {}^4I_{11/2}(Er^{3+}) \rightarrow {}^4F_{9/2}(Er^{3+}) + {}^4I_{15/2}(Er^{3+})$) and EBT ($^4S_{3/2}(Er^{3+}) + {}^2F_{7/2}(Yb^{3+}) \rightarrow {}^4I_{13/2}(Er^{3+}) + {}^2F_{5/2}(Yb^{3+})$) processes, resulting in an enhanced population of the $^4F_{9/2}$ and $^4I_{13/2}$ states. Since the population of the $^4F_{9/2}$ state results from the $^4I_{13/2}$ state of Er^{3+} ion via ET process: $^4I_{13/2}(Er^{3+}) + {}^2F_{5/2}(Yb^{3+}) \rightarrow {}^4F_{9/2}(Er^{3+}) + {}^2F_{7/2}(Yb^{3+})$, the increased population of the $^4F_{9/2}$ and $^4I_{13/2}$ states would lead to the enhanced red upconversion emission and the reduced green upconversion luminescence emission. Therefore, the intensity ratios of the green to red emission $R_{(g/r)}$ are increased with the reduced concentration of Yb^{3+} ions (Fig. 8).

Upconversion luminescence materials have been used to improve the efficiency of solar cell, such as lanthanide doped upconverting nanoparticles (UCNPs) [16]. Bulk upconversion luminescence glass obtains advantages: (1) it can enlarge the concentration of the doped rare earth ions in order to obtain high upconversion luminescence; (2) the bulk glass form can be mechanically fabricated; (3) it can be easily for the practical use. Thus, it will be very helpful in the application for solar cell. The NLZ6 has been applied in the DSSC, as shown in Fig. 9. The *I*–*V* characteristics of

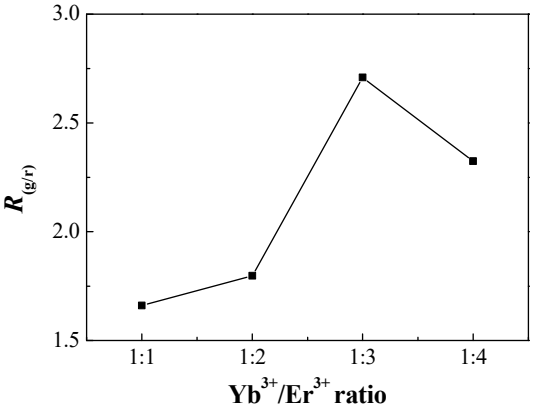

Fig. 8 Intensity ratio of the green emission to the red emission $R_{(g/r)}$ in NLZ*n* (*n* = 6, 7, 8, 9).

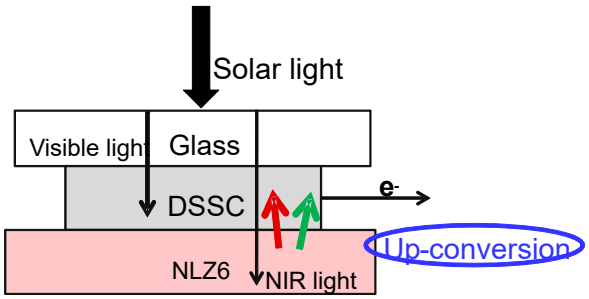

Fig. 9 Schematic illustration of NLZ6 applied in the DSSC, which can upconvert partial NIR light into red and green light, thus improving solar cell efficiency.

DSSC and DSSC with upconversion luminescence material NLZ6 are shown in Fig. 10. Light-to-electricity conversion efficiency (η) was obtained according to equation [27]:

$$\eta = J_{sc} V_{oc} FF / P_{in}$$

where J_{sc} is the short-circuit photocurrent density, V_{oc} is the open-circuit voltage, *FF* is the fill factor, and P_{in} is the incident radiation power. Compared with the control solar cell, V_{oc} of DSSC with NLZ6 glass is from 0.70 to 0.69 V, and J_{sc} increases from 13.63 to 13.96 mA/cm^2. *FF* is 0.67. The solar cell efficiency has been improved from 6.78% to 6.84%. It proves the potential application of upconversion luminescence glass in DSSC.

4 Conclusions

Niobium pentoxide glasses codoped with Er^{3+}/Yb^{3+} were fabricated by the aerodynamic levitation method with rapid cooling rate. All transparent samples

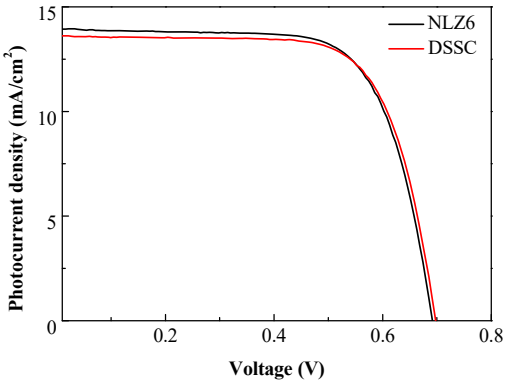

Fig. 10 Current–voltage (*I*–*V*) characteristics of DSSC without and with upconversion luminescence material NLZ6.

exhibited green and red upconversion emissions centered at 532, 547, and 670 nm. The sample with 1 mol% Er^{3+}/Yb^{3+} obtained the strongest upconversion emissions. The log*I*–log*P* plot of green emission indicates that the green emissions saturate at high pump power excitation, deviating from the low-power regime. The slope values become smaller in the green emissions for sample with different concentration of Er^{3+}/Yb^{3+} may be attributed to the ET process. After one-photon ET process, $^4I_{11/2} + {}^4I_{11/2} \rightarrow {}^4F_{7/2} + {}^4I_{15/2}$ process between the two neighboring Er^{3+} ions is responsible for the population of the $^4S_{3/2}/^4H_{11/2}$ states. The increased concentration of Yb^{3+} resulted in the increased red emission and reduced green emission for the increased rate of CR and EBT processes. The niobium pentoxide codoped with Er^{3+}/Yb^{3+} bulk glasses has been applied in the DSSC. V_{oc} increased from 0.69 to 0.70 V, and solar cell efficiency has been improved from 6.78% to 6.84%. The results indicate these upconversion luminescence material glass could be considered to be applied in DSSC to improve the efficiency of solar cell.

Acknowledgements

This work was financially supported by the National Natural Science Foundation of China (Grant Nos. 51671181, 51674232, and 51471158), Beijing Natural Science Foundation (No. 2152032), the Science and Technology Plan of Shenzhen City (Grant No. JCYJ20150827165038323), State Key Laboratory of New Ceramic and Fine Processing Tsinghua University (No. KF201417), the Open Funding Project of Key Laboratory of Photochemical Conversion and Optoelectronic Materials (TIPC in CAS), and the Instrument Developing Project of the Chinese Academy of Sciences (Grant No. YZ201520).

References

[1] Rodríguez-Rodríguez H, Imanieh MH, Lahoz F, *et al.* Analysis of the upconversion process in Tm^{3+} doped glasses for enhancement of the photocurrent in silicon solar cells. *Sol Energ Mat Sol C* 2016, **144**: 29–32.

[2] Tikhomirov VK, Rodriguez VD, Mendez-Ramos J, *et al.* Optimizing Er/Yb ratio and content in Er–Yb co-doped glass-ceramics for enhancement of the up- and down-conversion luminescence. *Sol Energ Mat Sol C* 2012, **100**: 209–215.

[3] Maji SK, Sreejith S, Joseph J, *et al.* Upconversion nanoparticles as a contrast agent for photoacoustic imaging in live mice. *Adv Mater* 2014, **26**: 5633–5638.

[4] Sarakovskis A, Krieke G. Upconversion luminescence in erbium doped transparent oxyfluoride glass ceramics containing hexagonal $NaYF_4$ nanocrystals. *J Eur Ceram Soc* 2015, **35**: 3665–3671.

[5] Chen D, Wan Z, Zhou Y, *et al.* Tailoring Er^{3+} spectrally pure upconversion in bulk nano-glass-ceramics via lanthanide doping. *J Eur Ceram Soc* 2016, **36**: 679–688.

[6] Dey R, Pandey A, Rai VK. The Er^{3+}–Yb^{3+} codoped La_2O_3 phosphor in finger print detection and optical heating. *Spectrochim Acta A* 2014, **128**: 508–513.

[7] Singh SK, Kumar K, Rai SB. Multifunctional Er^{3+}–Yb^{3+} codoped Gd_2O_3 nanocrystalline phosphor synthesized through optimized combustion route. *Appl Phys B* 2009, **94**: 165–173.

[8] Nyk M, Kumar R, Ohulchanskyy TY, *et al.* High contrast *in vitro* and *in vivo* photoluminescence bioimaging using near infrared to near infrared up-conversion in Tm^{3+} and Yb^{3+} doped fluoride nanophosphors. *Nano Lett* 2008, **8**: 3834–3838.

[9] Wang L, Yan R, Huo Z, *et al.* Fluorescence resonant energy transfer biosensor based on upconversion-luminescent nanoparticles. *Angew Chem Int Edit* 2005, **44**: 6054–6057.

[10] Zych E, Trojan-Piegza J, Kępiński L. Homogeneously precipitated Lu_2O_3:Eu nanocrystalline phosphor for X-ray detection. *Sensor Actuat B: Chem* 2005, **109**: 112–118.

[11] Rai VK, Pandey A, Dey R. Photoluminescence study of Y_2O_3:Er^{3+}–Eu^{3+}–Yb^{3+} phosphor for lighting and sensing applications. *J Appl Phys* 2013, **113**: 083104.

[12] Murthy KVR. Up-conversion phosphors synthesis and application in solar converters. *Int J Lumin Appl* 2013, **3**: 1–5.

[13] Furman JD, Warner AY, Teat SJ, *et al.* Tunable ligand-based emission from inorganic-organic frameworks: A new approach to phosphors for solid state lighting and other applications. *Chem Mater* 2010, **22**: 2255–2260.

[14] Chen Z, He S, Butt H-J, *et al.* Photon upconversion lithography: Patterning of biomaterials using near-infrared light. *Adv Mater* 2015, **27**: 2203–2206.

[15] Qiao R, Liu C, Liu M, *et al.* Ultrasensitive *in vivo* detection of primary gastric tumor and lymphatic metastasis using upconversion nanoparticles. *ACS Nano* 2015, **9**: 2120–2129.

[16] Yuan C, Chen G, Li L, *et al.* Simultaneous multiple wavelength upconversion in a core–shell nanoparticle for enhanced near infrared light harvesting in a dye-sensitized solar cell. *ACS Appl Mater Interfaces* 2014, **6**: 18018–18025.

[17] Ivanova S, Pellé F. Strong 1.53 μm to NIR–VIS–UV upconversion in Er-doped fluoride glass for high-efficiency solar cells. *J Opt Soc Am B* 2009, **26**: 1930–1938.

[18] Liu M, Lu Y, Xie ZB, *et al.* Enhancing near-infrared solar cell response using upconverting transparent ceramics. *Sol Energ Mat Sol C* 2011, **95**: 800–803.

[19] Lahoz F, Pérez-Rodríguez C, Hernández SE, *et al*. Upconversion mechanisms in rare-earth doped glasses to improve the efficiency of silicon solar cells. *Sol Energ Mat Sol C* 2011, **95**: 1671–1677.

[20] Ma X, Peng Z, Li J. Effect of Ta_2O_5 Substituting on thermal and optical properties of high refractive index

La_2O_3–Nb_2O_5 glass system prepared by aerodynamic levitation method. *J Am Ceram Soc* 2015, **98**: 770–773.

[21] Li J, Li J, Li B, *et al.* An upconversion niobium pentoxide bulk glass codoped with Er^{3+}/Yb^{3+} fabricated by aerodynamic levitation method. *J Am Ceram Soc* 2015, **98**: 1865–1869.

[22] Yoshimoto K, Masuno A, Inoue H, *et al.* Transparent and high refractive index La_2O_3–WO_3 glass prepared using containerless processing. *J Am Ceram Soc* 2012, **95**: 3501–3504.

[23] Pukhkaya V, Goldner P, Ferrier A, *et al.* Impact of rare earth element clusters on the excited state lifetime evolution under irradiation in oxide glasses. *Opt Express* 2015, **23**: 3270–3281.

[24] Li J, Ba G, Hu P, *et al.* Amorphous titanate nanospheres fabricated using contactless phase change process. *J Mater Chem* 2012, **22**: 9450–9454.

[25] Xiang H, Guan L, Peng Z, *et al.* Preparation of high refractive index La_2O_3–TiO_2 glass by aerodynamic levitation technique and effects of Bi_2O_3 substitution on its thermal and optical properties. *Ceram Int* 2014, **40**: 4985–4988.

[26] Nagashio K, Takamura H, Kuribayashi K. Containerless solidification of peritectic and eutectic ceramics using aero-acoustic levitator. *Mater Sci Forum* 2000, **329–330**: 173–178

[27] Liu Y, Lin H, Joanne TD, *et al.* Kinetics versus energetics in dye-sensitized solar cells based on an ethynyl-linked porphyrin heterodimer. *J Phys Chem C* 2014, **118**: 1426–1435.

[28] Zhao J. *Foundation of Material Science*. Dalian, China: DUT Press, 2010: 45.

[29] Shi L, Shen Q, Qiu Z. Concentration-dependent upconversion emission in Er-doped and Er/Yb-codoped $LiTaO_3$ polycrystals. *J Lumin* 2014, **148**: 94–97.

[30] Pan X, Yu J, Liu Y, *et al.* Thermal, mechanical, and upconversion properties of Er^{3+}/Yb^{3+} co-doped titanate glass prepared by levitation method. *J Alloys Compd* 2011, **509**: 7504–7507.

[31] Li D, Dong B, Bai X, *et al.* Influence of the TGA modification on upconversion luminescence of hexagonal-phase $NaYF_4:Yb^{3+},Er^{3+}$ nanoparticles. *J Phys Chem C* 2010, **114**: 8219–8226.

[32] Choi DH, Kang DH, Yi SS, *et al.* Up-conversion luminescent properties of $La_{(0.80-x)}VO_4:Yb_x,Er_{0.20}$ phosphors. *Mater Res Bull* 2015, **71**: 16–20.

[33] Marín-Dobrincic M, Sanz-García JA, Cantelar E, *et al*. $LiNbO_3:Yb^{3+}/Er^{3+}/Tm^{3+}$—power driven green to blue tenability. *Mater Lett* 2013, **96**: 63–66.